Biochimica et Biophysica Acta 1834 (2013) 46–52

Contents lists available at SciVerse ScienceDirect

Biochimica et Biophysica Acta

journal homepage: www.elsevier.com/locate/bbapap

Structure–activity relationship for enantiomers of potent inhibitors of *B. anthracis* dihydrofolate reductase

Christina R. Bourne [a,*], Nancy Wakeham [a], Baskar Nammalwar [b], Vladimir Tseitin [c], Philip C. Bourne [a], Esther W. Barrow [a], Shankari Mylvaganam [c], Kal Ramnarayan [c], Richard A. Bunce [b], K. Darrell Berlin [b], William W. Barrow [a,**]

[a] *Department of Veterinary Pathobiology, Center for Veterinary Health Sciences, Oklahoma State University, Stillwater, OK 74078, USA*
[b] *Department of Chemistry, Oklahoma State University, Stillwater, OK 74078, USA*
[c] *Sapient Discovery, San Diego, CA 92127, USA*

ARTICLE INFO

Article history:
Received 27 June 2012
Received in revised form 9 August 2012
Accepted 4 September 2012
Available online 20 September 2012

Keywords:
Antibiotic resistance
Bacillus anthracis
Dihydrofolate reductase
Dihydrophthalazine
Enantiomer
Racemate

ABSTRACT

Background: Bacterial resistance to antibiotic therapies is increasing and new treatment options are badly needed. There is an overlap between these resistant bacteria and organisms classified as likely bioterror weapons. For example, *Bacillus anthracis* is innately resistant to the anti-folate trimethoprim due to sequence changes found in the dihydrofolate reductase enzyme. Development of new inhibitors provides an opportunity to enhance the current arsenal of anti-folate antibiotics while also expanding the coverage of the anti-folate class. Methods: We have characterized inhibitors of *B. anthracis* dihydrofolate reductase by measuring the K_i and MIC values and calculating the energetics of binding. This series contains a core diaminopyrimidine ring, a central dimethoxybenzyl ring, and a dihydrophthalazine moiety. We have altered the chemical groups extended from a chiral center on the dihydropyridazine ring of the phthalazine moiety. The interactions for the most potent compounds were visualized by X-ray structure determination. Results: We find that the potency of individual enantiomers is divergent with clear preference for the *S*-enantiomer, while maintaining a high conservation of contacts within the binding site. The preference for enantiomers seems to be predicated largely by differential interactions with protein residues Leu29, Gln30 and Arg53. Conclusions: These studies have clarified the activity of modifications and of individual enantiomers, and highlighted the role of the less-active *R*-enantiomer in effectively diluting the more active *S*-enantiomer in racemic solutions. This directly contributes to the development of new antimicrobials, combating trimethoprim resistance, and treatment options for potential bioterrorism agents.

Published by Elsevier B.V.

1. Introduction

Bacteria affecting human health are increasingly acquiring antibiotic resistance [1]. All known strains of *Bacillus anthracis*, the causative agent of anthrax, encode for a dihydrofolate reductase (DHFR) enzyme that is not susceptible to trimethoprim, which is the only commercially available anti-DHFR therapy for bacterial infections [2–4]. Some strains of *B. anthracis* are Category A Select Agents, and they have been documented as previously engineered and weaponized by some countries [5]. This provides a unique advantage in terms of biodefense, as cellular functions not currently targeted by therapeutics are unlikely to be maliciously engineered.

DHFR inhibitors are an active and established area of development, and many recent efforts are using this target to respond to the problem of antibiotic resistance. Aside from the scaffold described herein and also previously by Basilea Pharmaceutica Ltd. [6,7], other anti-DHFR compounds under development include Iclaprim, being pursued by Acino Pharma [8], AR-709, pursued by Evolva [9], and 7-aryl-2,4-diaminoquinazolines, pursued by Trius Therapeutics [10]. A review of recent patent literature outlined antibacterial efforts targeting DHFR specifically for bacteria relevant to human health, including *Staphylococcus aureus*, *Pneumocystis carinii* and *B. anthracis* [11].

As part of our ongoing program to develop antimicrobials capable of targeting *B. anthracis* we have extended the previously reported dihydrophthalazine-based RAB1 series [2,12]. Completion of the X-ray crystal structure of *B. anthracis* DHFR complexed with RAB1 highlighted the long and deep hydrophobic pocket of ~600 $Å^3$ normally accommodating dihydrofolate as part of the catalytic addition of protons to form tetrahydrofolate [12]. This step is essential to bacterial metabolism, and inhibition leads to depletion of precursors needed for synthesis of nucleic acids [13]. Contacts between the protein and the diaminopyrimidine ring were conserved relative to

* Corresponding author. Tel.: +1 405 744 6737; fax: +1 405 744 5275.
** Corresponding author. Tel.: +1 405 744 1842; fax: +1 405 744 3738.
E-mail addresses: christina.bourne@okstate.edu (C.R. Bourne), bill.barrow@okstate.edu (W.W. Barrow).

1570-9639/$ – see front matter. Published by Elsevier B.V.
http://dx.doi.org/10.1016/j.bbapap.2012.09.001

known interactions of this site with substrate or other anti-folates [14–17]. These contacts include Glu28, of which an equivalent residue is present in all known DHFR enzymes, and Phe96, which has been implicated in mediating resistance to trimethoprim [14,18]. Overall the interactions between the protein and RAB1 were hydrophobic and included more than 20 other residues. The dihydrophthalazine moiety displayed shape complementarity to residue Leu55 and the dihydrophthalazine placement within the binding site triggered a conformational change of the side chains of Arg58 and in turn Met37. These observations provided evidence of specificity for bacterial versus human DHFR due to the terminal dihydrophthalazine moiety, as its length and volume could not be accommodated within the human DHFR binding pocket [12].

Original work on this series was carried out in conjunction with Basilea Pharmaceutica Ltd. The most promising modification was at a chiral carbon within the dihydropyridazine ring, but the chemical space that was explored was limited to linear alkyl or six-membered rings, with some extensions from these six-membered rings in only the ortho position [2]. RAB1 contains an *n*-propyl at this chiral carbon, and a preference for the *S*-enantiomer was visualized in the crystal structure [12]. This preference was mediated by the position of the terminal guanidino group of Arg58, which would sterically occlude the binding of the R-enantiomer at this position. Further, the position of Arg58 was solidified by hydrogen bonding to the carbonyl-linker of RAB1 either directly or via a water molecule. In the current work, we have continued these studies by further altering the group at this chiral carbon, which is located at the protein and solvent interface, determined the effect on potency, and compared this to in silico calculations as well as binary co-crystal structures available for the more potent compounds (Fig. 1).

2. Materials and methods

Chemical synthesis of inhibitors has been detailed in previous publications [12,19]; separation of enantiomers has also been reported [20]. Protein expression, purification and crystallization followed that described earlier [12]. Assessment of enzymatic activity and the minimum inhibitory concentrations (MIC) were also described previously [21]. Conversion of IC_{50} values to inhibition constant (K_i) values was achieved by using the Cheng–Prusoff equation with a determined K_M value of 16.3 μM (data not shown).

X-ray data for the *R*-isobutenyl and *R,S*-isobutyl complexes were collected at the Center for Advanced Microstructures and Devices, Baton Rouge, LA; these were indexed and scaled with HKL2000 [22]. The *R,S*-isobutyl data set was extremely weak and in many frames exhibited a split pattern of diffraction; this is reflected in the value of R_{sym} (Table 1). Data for the *R,S*-trifluoropropyl complex were collected at the University of Oklahoma, Norman, OK; these were indexed with iMosflm and scaled with SCALA [23,24]. Data for the *R,S*-phenyl and *R,S*-isopropyl complexes were collected at Oklahoma State University, Stillwater, OK, and were indexed and scaled with Saint and SADABS, as incorporated in the Proteum2 software suite [25]. Statistics for the processing and scaling of these data sets utilized Xprep [26], which reports that values of R_{sym} for all data, are causing an apparent increase relative to other data sets (for *R,S*-phenyl the overall value is 19.2%, and for *R,S*-isopropyl the overall value is 11.6%, see Table 1). Three-dimensional structures were isomorphous with the previous structure, PDB ID 3FL8 [12].

Refinement was carried out with Phenix [27] supplemented by the program Coot [28] for model visualization and manual building. When dual occupancy of enantiomers was identified, coordinates for the enantiomeric models were split into the portion sharing the same position and the portion showing different positions. Only the later portion was used to calculate occupancy. Figures were generated with the Chimera program from UCSF [29]. Model coordinates and structure factors have been deposited with the Protein Databank and accession codes are listed in Table 1. Atomic contacts between protein and ligand molecules were calculated with the Ligand–Protein Contacts server [30], assisted by calculations from the CASPp server [31].

Calculation of energy values upon complexation (ΔE) was performed with minimization algorithms from the SYBYL software suite (SYBYL 8.1, Tripos Certara Company) and with Monte-Carlo simulations performed with in-house software (Sapient Discovery). Starting models were based on the previously published 3FL8 structure with the *S-n*-propyl modification [12] or with the current structure 4ELH with the *R*-isobutenyl modification. All calculations utilized a 7 Å diameter sphere within the binding site for flexibility and minimization, and incorporated terms for van der Waals and electrostatic forces as well as

A

R1	K_i (SEM) nM	MIC[a] μg / mL	$\Delta E_{binding}$ S kcal / mol	$\Delta E_{binding}$ R kcal / mol	ΔΔE
propyl[b]	9.4 (0.5)	1 – 3	40.66	34.96	5.70
isopropyl[c]	13.2 (0.5)	1 – 2	40.08	34.78	5.30
trifluoropropyl[c]	9.4 (0.5)	1 – 2	40.96	36.00	4.96
isobutyl[c]	6.9 (0.5)	1 – 2	41.50	35.09	6.41
isobutenyl[c]	8.2 (0.5)	0.5	41.49	34.42	7.07
1-ethylpropyl	12.5 (0.5)	4 – 8	41.11	36.02	5.09
phenyl[c]	5.0 (0.6)	0.4 – 1.5	41.77	34.90	6.87
meta-fluorophenyl	4.8 (0.5)	2	41.93	35.68	6.25
para-fluorophenyl	6.4 (0.6)	1 – 2	41.60	35.23	6.37
para-methylphenyl	12.4 (0.5)	1 – 2	41.64	35.96	5.68
meta,meta'-dimethylphenyl	30.7 (0.6)	4 – 8	39.88	36.15	3.73
ortho-methylphenyl	11.2 (0.5)	8	39.98	35.82	4.16
benzyl	41.8 (0.5)	8	40.10	34.97	5.14
para-methylbenzyl	28.0 (0.6)	4 – 8	41.09	35.02	6.07
para-methoxybenzyl	93.4 (0.5)	8 – 16	39.86	35.09	4.78
para-trifluoro-methoxybenzyl	> 2,100	4	41.48	34.78	6.69

B

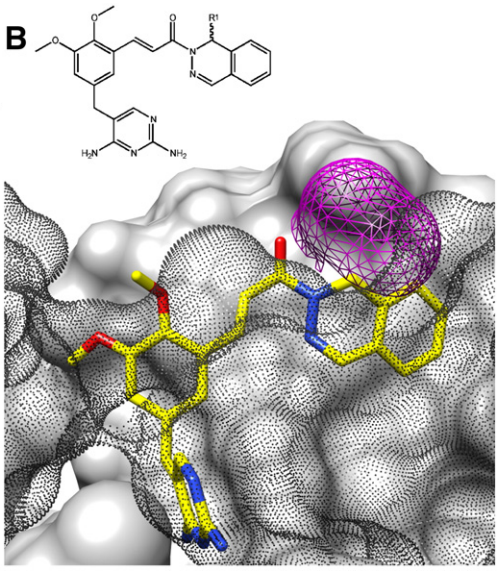

Fig. 1. Modifications at "R1" are designed to modulate the potency with interactions at the protein's interface with solvent. A) K_i (Standard Error of the Mean, SEM) and MIC values were determined with racemic mixtures of inhibitors; calculation of the energy of binding for individual enantiomers is given, and ΔΔE is the difference in energetics of enantiomers. a. MIC values have been published [19]. b. Values for the *n*-propyl modification IC_{50}, MIC and binary co-crystal structure have been previously published [12]. c. Binary co-crystal structures presented in current work. B) Two dimensional depiction and view of the inhibitor in the binding site. The protein has a gray van der Waals surface, with the proximal region depicted as transparent dots to permit visualization of the inhibitor buried within the site. The magenta wire cage indicates the position of the R1 inhibitor modifications.